TEKTONIKA

Mechanical Analysis of Fault Slip Rate Sites within the San Gorgonio Pass Region, Southern California USA

Jennifer Hatch [1], **Michele Cooke** *[1], **Hanna Elston** [1]

[1]Department of Earth, Geographic and Climate Sciences, University of Massachusetts, Amherst MA, USA

Abstract Earthquake hazard assessments rely on observations from the field and geophysical data that provide fault slip rate estimates at specific sites and inform the geometry of active faults; however, uncertainty remains for both slip rate and geometry. Furthermore, incompatibilities between inferred fault geometry and geologic slip rates arise within crustal deformation models where model and geologic slip rates disagree. The impact of these incompatibilities may be local to sites or have wider effect on the fault system deformation. Here, we investigate the roles of structural position of sites and uncertainty of slip rates using three-dimensional mechanical models that simulate deformation across many earthquake cycles along southern San Andreas fault near the San Gorgonio Pass in California. Within the models, the impact of strike-slip rate sites on the fault system depends on their structural positions. Slip rates at sites along short and segmented faults has lesser impact on the slip along the fault system than either slip rates at sites along longer faults or at sites within fault branches. Consequently, inaccuracies in the slip rate estimates used for seismic hazard assessment may have differing impacts on the fault system depending on location and structural position of the slip rates. Fault branches along strike-slip faults warrant detailed investigation not only because these areas have high spatial variability of slip rate and accrue nearby off-fault deformation but also because changes in slip rates along branches has larger impact on deformation along fault system than other sites. Lack of data or large uncertainty in slip rate data from fault branches can affect our ability to accurately assess seismic hazard of the region.

Executive Editor:
Craig Magee
Associate Editor:
L. Muniz Pichel
Technical Editor:
Mohamed Gouiza

Reviewers:
Sam Wimpenny
Rebecca Bell

Submitted:
22 January 2023
Accepted:
13 April 2023
Published:
9 June 2023

1 Introduction

While geologic evidence for slip rates along active faults provides critical information for constraining seismic hazard assessments (*Field et al.*, 2015; *Morell et al.*, 2020, e.g.,), uncertainties in slip rate estimates that derive from a variety of sources can be large enough (> 10 mm/yr) to compromise the accuracy of our hazard estimates. In the face of these large uncertainties, collecting slip rate data from additional sites provides one way to improve constraints on active slip partitioning. However, in regions of multiple active faults with complex evolving geometry, where slip rates can vary both in space and in time (e.g., *Elston et al.*, 2022; *McGill et al.*, 2021; *Zinke et al.*, 2017), this approach can yield slip rates that are inconsistent with each other. One such region is where the southern San Andreas fault in southern California forms a restraining bend in the San Gorgonio Pass region (SGPr) (Figure 1). Because earthquakes along the San Andreas fault pose a great risk to the highly populated cities of southern California, the region has been the focus of many geologic investigations, and these studies have produced many slip rate estimates on the San Andreas fault through the SGPr (Figure 1). However, the geologic slip rate estimates to date do not present a consistent interpretation of slip rate distribution along the strands and segments of the San Andreas fault.

For example, debate persists on the relative activity of the Mill Creek and Mission Creek strands, which provide a northern path for rupture through the SGPr (Figure 1; *Blisniuk et al.*, 2021; *Fosdick and Blisniuk*, 2018; *Gold et al.*, 2015; *Kendrick et al.*, 2015). *Kendrick et al.* (2015) used reconstructed drainage segments across the Mill and Mission Creek strands (site B in Figure 1) to show that both strands, while active in the past, have been inactive for ~100 ka. However, a provenance study in this same area by *Fosdick and Blisniuk* (2018) suggests that these strands are currently active. Farther to the east along the Mission Creek fault, two sites within 5 km of each other (sites C and 9; Figure 1) have slip rates that differ by >10 mm/yr; 19.6–23.6 mm/yr at site C (*Blisniuk et al.*, 2021) and 10–14 mm/yr at site 9 (*Muñoz Zapata*, 2017). These slip rates are averaged over different time periods (Table 1), which complicates their direct application to current seismic hazard assessment. Long term slip rates from very young deposits (fewer than five earthquakes) may be impacted by earthquake cycles (e.g., *Styron*, 2019) and older deposits have in-

*✉ cooke@umass.edu

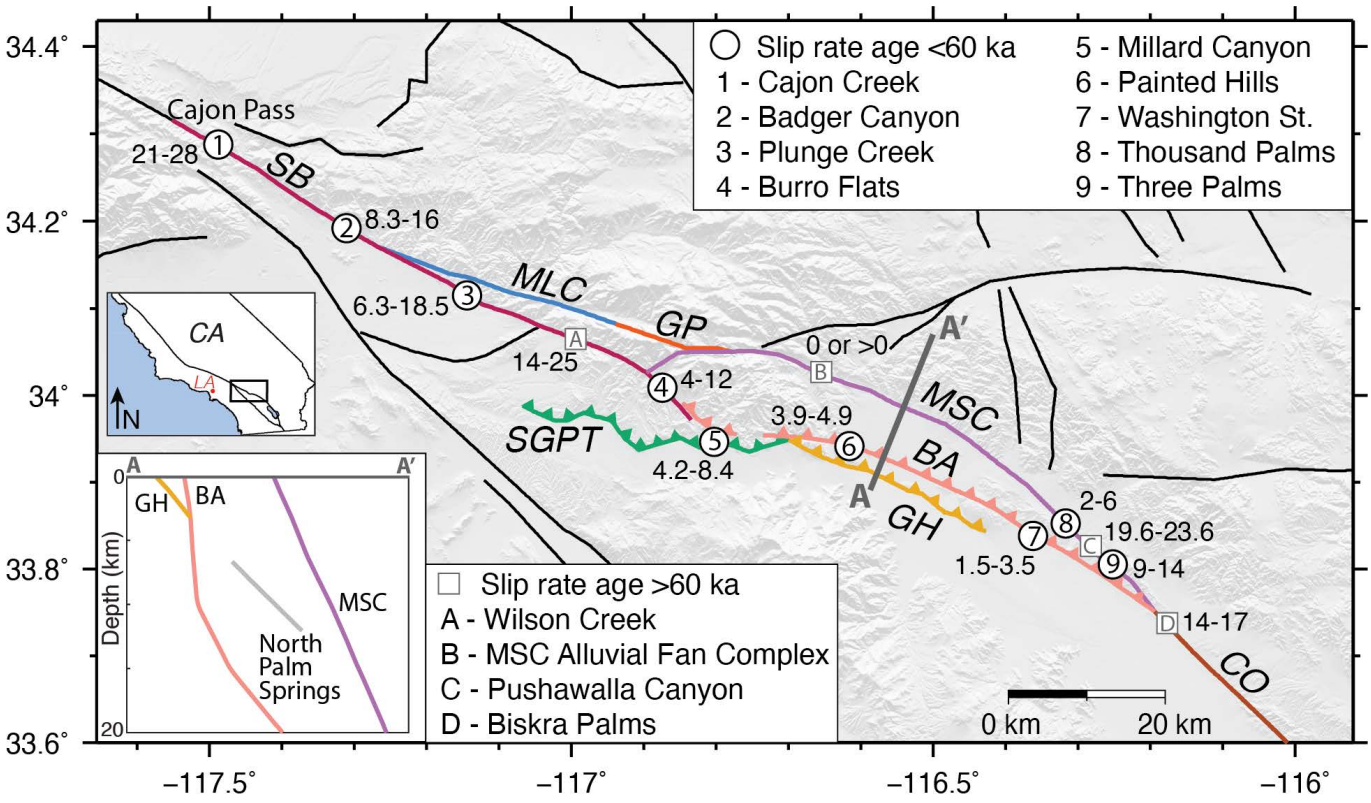

Figure 1 – The surface traces of modelled faults overlain on a digital elevation map (DEM). Different trace colors indicate the specific fault segments. Numbers in circles show the location of slip rate sites that we use to constrain the model slip rate. Letters in squares indicate the location of slip rate sites that we do not use to constrain the model slip rate. The bottom left inset shows the cross-section profile along the A-A′ line (dark gray). The top left inset shows the region of interest (black rectangle) on a map of southern California. Table 1 lists the name and citation for all the slip rate sites. BA: Banning; CO: Coachella; GH: Garnet Hill; GP: Galena Peak; MLC: Mill Creek; MSC: Mission Creek; SB: San Bernardino; SGPT: San Gorgonio Pass Thrust.

Table 1 – Data from geologic strike-slip rate sites.

Site	Name	Age	Dextral slip rate (mm/yr)	Citation	Used here to constrain model slip rate?
1	Cajon Creek	~14 ka	21-28	*Weldon and Sieh* (1985)	yes
2	Badger Canyon	13-15 ka	11.8 $^{+4.2/-3.5}$	*McGill et al.* (2021)	yes
3	Plunge Creek	10.5 ka	6.3–18.5	*McGill et al.* (2013)	yes
A	Wilson Creek	~14 ka	14-25	*Harden and Matti* (1989)	no; non-robust age
4	Burro Flats	~4 ka	~4–12	*Orozco* (2004)	yes
5	Millard Canyon	~8ka	5.2 $^{+2.4/-1.4}$	*Heermance and Yule* (2017)	yes
6	Painted Hills	~6 ka	~3.9–4.9	*Gold et al.* (2015)	yes
7	Washington St.	~6 ka	~1.5–3.5	*Blisniuk et al.* (2021)	yes
B	Mission Creek Alluvial Fan Complex	~100 ka	0 orc 0	*Kendrick et al.* (2015); *Fosdick and Blisniuk* (2018)	not constrained in *Active Northern Pathway* model
8	Thousand Palms	~500 years	2–6	*Fumal et al.* (2002)	Lower limit
C	Pushawalla Canyon	~90 ka	19.6–23.6	*Blisniuk et al.* (2021)	no; age 16 ka
9	Three Palms	2.6–6.4 ka	9–14	*Muñoz Zapata* (2017)	yes
D	Biskra Palms	~50 ka	14–17	*Behr et al.* (2010)	no; age 16 ka

creasing vulnerability for recording temporal variation in slip rates (e.g., *Rittase et al.*, 2014; *Hatem et al.*, 2020; *Elston et al.*, 2022; *Zinke et al.*, 2017). An interesting outcome of having abundant slip rate data is that inconsistency between slip rates decreases our confidence in our estimates of current fault activity along the southern San Andreas fault more than if we had just one slip rate; this is similar to the conundrum of having several clocks tell you different times.

Crustal deformation models provide a powerful tool for testing the mechanical consistency of slip rate estimates along faults within complex networks. We can test plausible fault configurations by comparing results of alternative mechanical models with geologic slip rates, uplift, and/or geodetic data (e.g., *Beyer et al.*, 2018; *Cooke and Dair*, 2011; *Fattaruso et al.*, 2014; *Herbert and Cooke*, 2012). For example, *Beyer et al.* (2018) find that two among six plausible configurations of the San Andreas fault through the SGPr fit

well the available geologic slip rates. Crustal deformation models can also highlight regions that would benefit from further investigation. Kinematic compatibility of a fault system describes how deformation is partitioned through the system (*Gabrielov et al.*, 1996; *Hatem et al.*, 2015), and its analysis can highlight regions where long-term fault slip rates are incompatible with the interpreted fault geometry. If interpreted fault geometries and slip rates are kinematically incompatible, such as fast slip rates through a sharp fault bend, deformation that cannot be effectively accommodated as fault slip results in local off-fault deformation that impacts the fault slip budget. Because slip along faults may not sum to the regional loading in these regions of high incompatibility, these regions require additional data to better characterize partitioning of active deformation.

The abundant slip rate data available from along the geometrically complex southern San Andreas fault (Figure 1) provides an ideal scenario to assess the relative impact of different slip rate sites on the partitioning of slip along the fault system. While some fault irregularities may only produce local off-fault deformation and persist throughout fault evolution (*Hatem et al.*, 2017), other incompatibilities between fault geometry and slip rate may have great impact on slip rates throughout the fault system and promote reorganization of the fault system (e.g., *Cooke et al.*, 2020; *Fattaruso et al.*, 2016). By assessing the locations along the fault system with the greatest influence on slip rates, we can better understand the potential impact of slip rate and fault geometry uncertainties and inaccuracy on our seismic hazard estimates.

In this study, we use three-dimensional Boundary Element Method models that simulate deformation over many earthquake cycles to investigate the compatibility of interpreted fault geometry with interpreted slip rates through the SGPr (Figure 1). Rather than letting faults slip everywhere in response to tectonic loading as done with many previous models (e.g., *Beyer et al.*, 2018), here in addition to allowing slip in response to tectonic loading, we prescribe geologic slip rates at the sites of the investigation. This allows the models to incorporate both interpreted slip rates and fault geometry at the same time so that we can assess their compatibility. To explore the impact of slip rate uncertainties, we investigate a second suite of models that apply 1 mm/yr to each of the slip rate sites independently to assess how slip at different sites impacts deformation elsewhere on the fault system due to variations in their structural position. The models provide a way to assess the sensitivity of different structural positions to uncertainties in slip rate data. The model results show that changes to slip rates at sites along fault branches has larger impact on deformation of the fault system than sites at other structural positions.

2 Geometry and Slip Rates of the Southern San Andreas Fault

Within the San Gorgonio Pass region (SGPr), the southern San Andreas fault forms a left-stepping restraining bend and becomes geometrically complex, with multiple active fault strands and a complex slip history (Figure 1 *Matti et al.*, 1985; *Matti and Morton*, 1993). In this section, we describe the interpreted geometry and records of recent slip rate along both the southern and northern strands of the San Andreas fault (Table 1). The San Andreas fault geometry used in this study primarily follows that of the Southern California Earthquake Center Community Fault Model (CFM) v. 5 (*Plesch et al.*, 2007; *Shaw et al.*, 2015) with exceptions noted below. Sites with slip rates that are either not well constrained or older than 40 ky are given a letter site name rather than a number and the slip rates estimates from these sites with older records that may record temporally varying slip rate are not used to constrain the models.

Dextral slip rates consistently decrease from north to south along the San Bernardino strand of the San Andreas fault from Cajon pass to where the strand approaches the San Gorgonio Pass thrust. At Cajon Creek the San Bernardino strand shows 21-28 mm/yr slip from 14 ka geomorphic features (site 1; *Weldon and Sieh*, 1985). The next three sites to the south constrain slip rates from offsets of 10–16 ka alluvial fans with 8.3–16 mm/yr at Badger Canyon (site 2; *McGill et al.*, 2021), 7–17 mm/yr dextral slip at Plunge Creek (site 3; *McGill et al.*, 2013) and 14–25 mm/yr at Wilson Creek (site A; *Harden and Matti*, 1989). The fan age at Wilson Creek site is an estimate rather than a measurement, which results in a large slip rate range. The southernmost slip rate site on the San Bernardino strand has 4–12 mm/yr slip rate recorded by offset of a ~4 ka alluvial fan at Burro Flats (site 4 *Orozco*, 2004).

Active slip along the southern pathway of the San Andreas fault within the SGPr occurs along the San Gorgonio Pass thrust, Garnet Hill strand, and Banning strand (Figure 1). The San Gorgonio Pass thrust is a north-dipping thrust fault that intersects the Earth's surface with a scalloped trace (e.g., *Matti and Morton*, 1993; *Matti et al.*, 1985; *Yule and Sieh*, 2003). The San Gorgonio Pass thrust has offset ~8 ka terraces to record a dextral-oblique slip rate of $5.7^{+2.7/-1.5}$ mm/yr at Millard Canyon (site 5; *Heermance and Yule*, 2017). This net slip rate resolves to $5.2^{+2.4/-1.4}$ mm/yr dextral slip and $2.4^{+1.1/-0.6}$ of reverse slip To the east of Millard Canyon, the north-dipping Garnet Hill and Banning strands are nearly parallel in strike and have several different interpreted subsurface geometries (*Fuis et al.*, 2017; *Plesch et al.*, 2007; *Yule and Sieh*, 2003). For this study, we follow the interpretations of *Fuis et al.* (2017) that the Garnet Hill strand is only active in the footwall of the Banning strand (Figure 1). While the Garnet Hill strand does not offer geomorphic features that can provide slip rate estimates, the parallel Banning strand offsets ~6 ka alluvial fans at both its western and eastern ends. The fan at Painted Hills

records 3.9–4.9 mm/yr dextral slip (site 6; *Gold et al.*, 2015) and the fan at Washington Street, near the intersection of the Banning strand with Mission Creek strand, records 1.5–3.5 mm/yr dextral slip (site 7; *Blisniuk et al.*, 2021).

The northern slip pathway of the San Andreas fault consists of the Mill Creek, Galena Peak, and Mission Creek strands (Figure 1). While the northern pathway was active in the past and served as the primary structure of the San Andreas fault in this region, recent activity of these vertical faults remains debated (e.g., *Beyer et al.*, 2018; *Blisniuk et al.*, 2021; *Fosdick and Blisniuk*, 2018; *Kendrick et al.*, 2015). Here, we include the Galena Peak strand as part of the northern pathway as it connects the Mill Creek strand and western part of the Mission Creek strand (e.g., *Dibblee*, 1964; *Kendrick et al.*, 2015; *Matti and Morton*, 1993). This active fault configuration allows slip to by-pass Upper Raywood Flats where *Kendrick et al.* (2015) found no evidence of slip in the past 100 ka. *Beyer et al.* (2018) found that among six plausible configurations of the San Andreas fault strands, the configuration that includes the Galena Peak strand matches the available geologic slip rates as well as the model without an Active Northern Pathway for slip through the San Gorgonio Pass.

Researchers report differing degrees of recent activity along the Mill Creek and Mission Creek strands west of the Galena Peak strand to the location just west of the A-A' transect within Figure 1. One study of the Mission Creek alluvial complex suggests that neither the Mission Creek nor Mill Creek faults have slipped at this location for 100 ka (site B; *Kendrick et al.*, 2015). In contrast, a sedimentary provenance study of modern drainages just a few kilometers away suggests that the Mission Creek fault may accommodate most of the deformation in the region (*Fosdick and Blisniuk*, 2018). To the east of the A-A' transect within Figure 1, the Mission Creek strand shows abundant evidence for slip but with a wide range of dextral slip rates. Within the Indio Hills, channel offsets at Pushawalla Canyon show high dextral slip rates of 19.6-23.6 mm/yr over the past ~90 ka (site C; *Blisniuk et al.*, 2021), consistent with active slip along the northern pathway through the SGPr. However, these channels do not record recent slip rates within the past 16 ka. A few kilometers south from Pushawalla Canyon at Three Palms, a young 2.6–6.4 ka alluvial fan shows much lower slip rate of 9–14 mm/yr dextral slip along the Mission Creek strand (site 9; *Muñoz Zapata*, 2017). A few kilometers north of Pushawalla, offset channels trenched across the Mission Creek fault at Thousand Palms recorded two slip events within the last 500 years that give slip rates of 2–6 mm/yr (site 8; *Fumal et al.*, 2002). Because trenches can miss expressions of slip along fault splays outside of the trench, we consider this a minimum slip rate for the Thousand Palms site.

The Banning and Mission Creek strands merge into the Coachella segment of the San Andreas fault just south of the Indio Hills (Figure 1). The Coachella segment dips to the northeast (e.g., *Fattaruso et al.*, 2014; *Fuis et al.*, 2017; *Lin*, 2013; *Lindsey and Fialko*, 2013) and continues southward from the Indio Hills to the eastern shore of the Salton Sea. Near the Indio Hills, the Mission Creek strand and the Coachella segment dip 5–10 degrees shallower in the Fuis-based models than in the CFM-based models due to changes in the geometry of the Banning strand. This geometry honors the interpretations of *Fuis et al.* (2017) for the Banning, Garnet Hill and Mission Creek strands to the north of Palm Springs and for the Coachella segment to the south of the Indio Hills. Just south of the junction with the Banning and Mission Creek, the Coachella segment shows evidence from 50 ka alluvial fans for a preferred rate of 14-17 mm/yr at Biskra Palms (site D; *Behr et al.*, 2010).

3 Methods

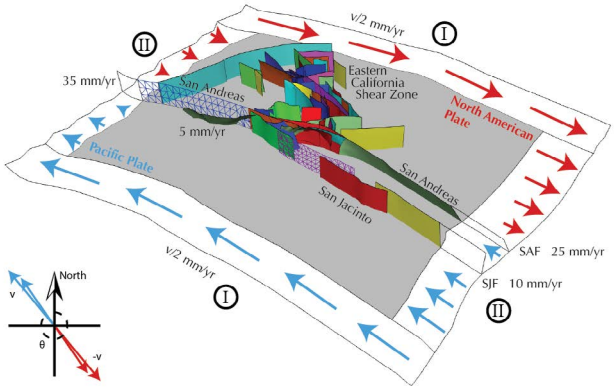

Figure 2 – Oblique view of the model setup taken from Beyer et al. (2018). Tectonic loading is prescribed far from the investigated faults at the boundaries of the model base. Zone of applied loading is much wider than shown here. Fault slip rates are prescribed at the distal end of faults that extend beyond the model boundaries. Faults within the model slip freely in response to both tectonic loading and fault interaction. A range of plate velocities and orientations account for uncertainty in tectonic loading. SAF: San Andreas fault; SJF: San Jacinto fault.

We evaluate the impact of slip rates and sites along faults within the San Gorgonio Pass region (SGPr) on deformation within the southern San Andreas fault system using Poly3D, a quasi-static, three-dimensional Boundary Element Method code. Poly3D calculates stresses and displacements throughout the model domain by solving the linear-elastic equations of continuum mechanics (*Crider and Pollard*, 1998; *Thomas*, 1993). To incorporate fault discontinuities within the half-space continuum, Poly3D uses triangular elements built from angular dislocation solution of *Comninou and Dundurs* (1975). In addition to detailed three-dimensional representation of faults described in Section 2, the models incorporate the San Jacinto fault and faults of the Eastern California Shear Zone based on the Community Fault Model version 5 (Figure 2). Modifications to the Community Fault Model representation have improved

the match of model slip rates to geologic slip rates; we include these modifications of the Eastern California Shear Zone described by *Herbert et al.* (2014) and of the Coachella segment described by *Fattaruso et al.* (2014). We remeshed the Community Fault Model for more uniform element size and we iteratively refined the mesh to reduce model artifacts that arise when the faults slip.

For the mesh, faults are discretized into triangular elements that can replicate complex fault geometries within a linear-elastic and otherwise homogeneous half-space (Figure 2). Within the SGPr, the average element size is 4 km, allowing for the models to capture fault irregularities as small as ~10 km. Following *Marshall et al.* (2009), we extend the faults of the CFM down to a horizontal basal crack that is freely slipping at 35 km depth to simulate distributed deformation below seismogenic depths. This adaptation allows us to simulate long-term deformation without the fault slip rates going to zero at the base of the CFM-defined faults. Furthermore, we do not consider impacts of heterogeneous and/or anisotropic rock properties. Over multiple earthquake cycles, fault geometry provides a first-order control on deformation patterns (e.g., *Dawers and Anders*, 1995; *Fay and Humphreys*, 2005; *Herbert and Cooke*, 2012).

Within the unconstrained models, the faults throughout the model slip in response to both the tectonic loading and fault interaction. Because fault slip accumulates during earthquake events, the dynamic strength during slip rather than the static strength at the start of the slip event captures fault slip over many earthquake cycles. The zero shear traction applied to the modeled faults is consistent with low dynamic strength of faults during rupture (e.g., *Goldsby and Tullis*, 2011; *Di Toro et al.*, 2006). Tectonic loading is prescribed far from the investigated faults at the base of the model, following *Herbert and Cooke* (2012) to simulate plate motions that are geodetically constrained as 45–50 mm/yr at 320–325° (e.g., *DeMets et al.*, 2010). Following *Beyer et al.* (2018), we also implement an iterative technique that uses a correction ratio for successive iterations to ensure a uniform applied tectonic velocity parallel to the plate boundary (sides labeled I on Figure 2) and a linear gradient in the tectonic loading across the plate boundary adjacent to active faults (sides labeled II on Figure 2). This technique provides applied velocities that are within ~1% of the desired tectonic loading.

To prevent slip from artificially going to zero on faults that extend outside our model area (i.e., the San Andreas, San Jacinto, and Cucamonga-Sierra Madre fault systems), we prescribe slip rates to patches of these faults at the edge of our model. For the San Andreas fault, we apply 35 mm/yr dextral slip (*Weldon and Sieh*, 1985) at the northwestern edge of the model. At the southeastern edge of the model, we apply 25 mm/yr and 10 mm/yr dextral slip to the San Andreas and San Jacinto faults, respectively (e.g., *Becker et al.*, 2005; *Fay and Humphreys*, 2005; *Meade and Hager*, 2005; *Sharp*, 1981). Deformation within the SGPr is not significantly impacted by variations in the partitioning of slip rates between the San Andreas and San Jacinto faults at this model edge because slip rates primarily respond to interaction among complex faults within the SGPr (Fattaruso et al., 2014). Finally, we apply 1.6 mm/yr reverse slip (*McPhillips and Scharer*, 2018) to the western edge of the modeled Cucamonga fault to account for deformation along the Sierra Madre fault, which is not included in our model.

Because of the ongoing debate on the recent activity of the Mill Creek strand, we assess two alternative active fault configurations. Due to the low strength applied to faults in the models, all faults will slip, which means that inactive faults need to be either removed or prescribed zero slip. The first fault configuration model considers the northern slip pathway to be inactive through the SGPr; the model does not include the Mill Creek or Galena Peak strands and only allows slip along the Mission Creek strand southeast of the transect A-A' on Figure 1. The second model expands from the first fault configuration and incorporates active Mill Creek and Galena Peak strands as well as the entire Mission Creek strand (Figure 1). We refer to these two fault configurations as the Inactive Northern Pathway and the Active Northern Pathway models, respectively.

3.1 Impact of Slip Rates and their Uncertainty

To assess the impact of site specific slip rates and their uncertainty on slip elsewhere within the fault system, we compare the fault slip rates and off-fault deformation of models with both unconstrained and constrained slip rates. Within the first set of unconstrained models, we allow the faults everywhere in the model to slip freely in response to tectonic loading and fault interaction. In this first model, the slip rates are mechanically consistent with the fault geometry. For example, if the active fault configuration has a sharp change in fault strike, the slip rate will slow around this kink. However, some of the resulting slip rates may fall outside of the slip rate limits determined from geologic information. A mismatch in slip rates can arise from inaccuracies of either the model or the geologic interpretation. At any one site, a combination of factors may contribute to the uncertainty of the local slip rate. Here, we explore the impact of these slip rate mismatches on the fault system, regardless of the source of the mismatch. To do this we investigate a second set of constrained models, where we limit the slip rates at geologic sites within the models to within the geologic range. At each slip rate site along the fault, the prescribed slip rate patch is ~2 km by 2 km, just below the surface trace of the fault. Locations along the faults between the prescribed slip rate sites freely slip in response to tectonic loading, fault interaction, and the effects of prescribed slip patches.

Because geologic investigations produce a range of possible slip rates, we allow for a variety of slip rates at each site of geologic investigation in the model. In the absence of probability density functions for the slip rates, we treat the geologic slip rate as having uniform ("box car") probability within the published range. If the slip rates from the unconstrained model lie outside of the geologic range, then we prescribe the slip rate at the site to be either the upper or lower limit of the geologic slip rate range. If the slip rate in the unconstrained model is closer to the upper bound then we prescribe this slip rate at the site, otherwise we prescribe the lower bound slip rate at the site. Prescribing the geologic slip rate limit honors the geologic observation while also minimizing the deviation from the slip rate that is mechanically consistent with the interpreted active fault geometry (the unconstrained slip rate). Reducing the slip rate mismatch in the model aligns the model with the geologic data but does not inform the source of the mismatch.

Because some sites have uncertain recent slip rates, we either exclude them or limit their role within the constrained models (Table 1). The alluvial fan age at the Wilson Creek (site A) uses qualitative soil chronology rather than modern dating techniques (*Harden and Matti*, 1989). Because of this uncertainty, we include the slip rate for comparison but do not constrain the model to fit this slip rate. We also exclude slip rate constraints on the Mission Creek strand at the Mission Creek Alluvial Fan Complex (site B) within the Active Northern Pathway model because interpretations of recent slip along this portion of the fault (*Fosdick and Blisniuk*, 2018) do not provide rates. The *Kendrick et al.* (2015) interpretation of zero slip rate at site B is explicitly considered within the Inactive Northern Pathway model. The slip rate from the Thousand Palms trench (site C) may not include nearby fault strands (*Fumal et al.*, 2002); we use the reported range as only a lower limit for dextral slip rates. Slip rates from the Pushawalla Canyon (site C) and Biskra Palms (sites C) are based on > 60 ka alluvial fans (*Behr et al.*, 2010; *Blisniuk et al.*, 2021). Because the activity among fault strands in the SGPr has shifted over the past 100 ka, strands that were active 60 ka may have different activity now (e.g., *Kendrick et al.*, 2015). Laboratory experiments confirm that restraining bends with greater than 20° restraining bend angle, such as the SGPr, are unstable and generate new faults segments (*Cooke et al.*, 2013; *Hatem et al.*, 2015) and slip rates on some bends can vary on time spans of ~50 ka (*Elston et al.*, 2022). Because of the inferred shifts in activity over the last ~100 ka for the SGPr, we only use slip rates from offset of features younger than ~40 ka to constrain the models that simulate current fault slip patterns.

We assess the kinematic incompatibility of the two fault configurations (Inactive and Active Northern Pathway) for both the unconstrained and constrained models by calculating maps of the off-fault deformation. We assess the net strain rate, defined as the sum of the vorticity rate and the divergence rate derived from the velocity field at the top surface of the model half-space. The vorticity captures the distortion along and off of faults while divergence captures dilatational strain. In order to investigate the off-fault deformation, we exclude net strain rate information within 1 km from all active faults. We compare the resulting off-fault strain rate pattern, the mean net strain rate across the region and the uplift pattern to those of the unconstrained models. The spatial patterns of deformation reveal regions where geologic slip rates are incompatible with interpreted fault geometry, while the spatial average of the net strain rate provides a metric for the relative overall kinematic compatibility of the system. Because the model does not include isostacy, we correct the uplift rates of the BEM model using a model of elastic flexure of the crust that reduces amplitude and increases wavelength of uplift (e.g., *Cooke and Dair*, 2011; *Fattaruso et al.*, 2014, 2016). Here we use a mantle density of 4500 kg/m^3, crustal density of 2700 kg/m^3, and a flexural rigidity of the crust of 2x10^{23} Pa·m^3.

3.2 Assessing Impact of each Slip Rate Site on the System

Due to their structural position, some sites may have a stronger influence on slip rates along the fault system than other sites. While the kinematic efficiency analysis highlights regions of the model where fault geometry is incompatible with geologic slip rates, those findings do not inform the role of each site on the slip distribution within the system. We assess the sensitivity of individual sites by exploring the response of the fault system to 1 mm/yr of dextral strike slip applied at each of the sites independently. The influence factors report the change in slip rate at all other sites due to the applied 1 mm/yr at each site. Within the elastic model, the values of slip rate everywhere in the model scale linearly to the applied slip rate; we apply 1 mm/yr to all sites to allow direct comparison of site impact and to facilitate normalizing the slip rate uncertainties. To assess the impact along stretches of fault between the slip rate sites, we also calculate slip rate impact factors by integrating the slip along the fault system that results from applying 1 mm/yr at each site.

3.3 Results

To assess the roles of fault geometry and slip rate constraints, we present fault slip rates and off-fault deformation through the San Gorgonio Pass region (SGPr) for Inactive Northern Pathway and Active Northern Pathway models with unconstrained and constrained slip rates. Sites without reliable and young (< 40 ka) slip rates (sites A, B, C and D) are not constrained within the models but are considered within the analysis of site impact.

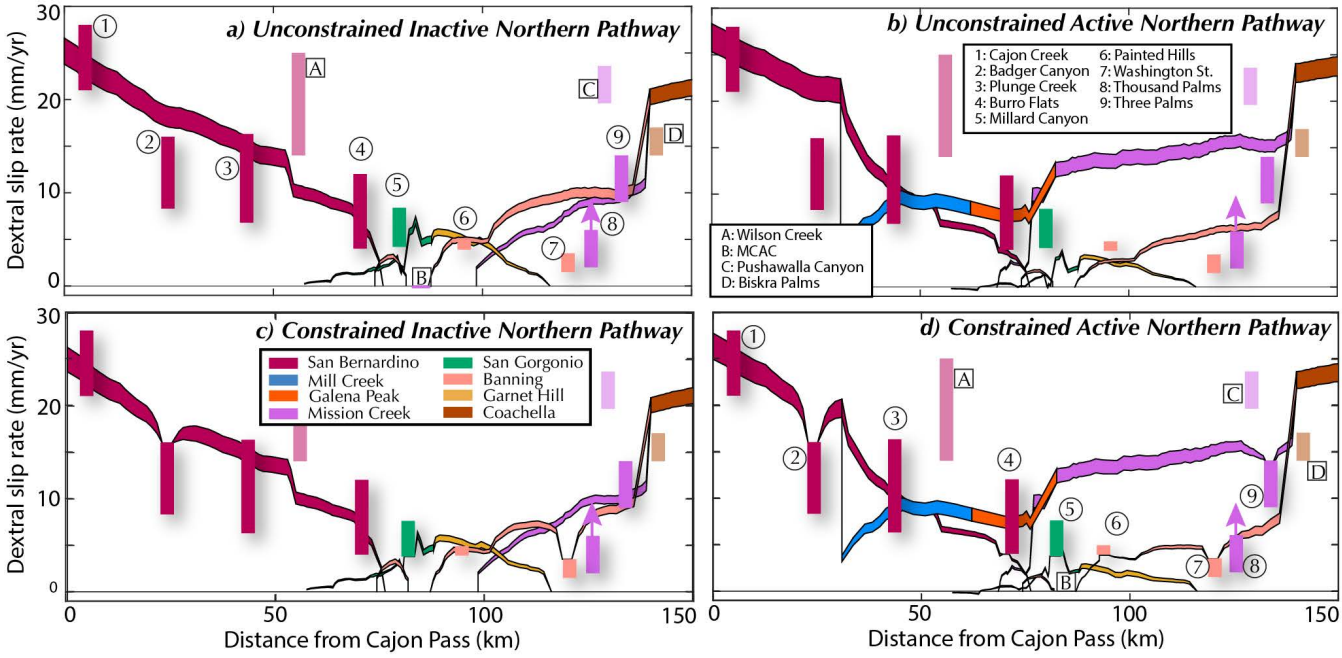

Figure 3 – Dextral slip rates along strands of San Andreas fault at the upper surface of the model. Vertical bars show the geologic slip rates at sites labeled in Figure 1; bars with lighter hues are not used for the model assessment. Upward pink arrow indicates that slip rate may exceed the reported range at Thousand Palms. The shaded bands show the range of modeled strike-slip faults for the various applied tectonic loading. **a)** and **b)** show results from the unconstrained models with and without an Active Northern Pathway for slip. The Inactive Northern Pathway model overlaps more geologic slip rates than the Active Northern Pathway model. **c)** and **d)** show results for the constrained model where we prescribed strike slip rate to fit within the geologic ranges at sites with robust estimates of slip rate within the past 40 k years.

3.4 Surface Slip Rates through the San Gorgonio Pass Region

Forward numerical models that simulate tectonic loading can provide slip rate estimates along the entire fault surface including at the sites of geologic slip rate investigations. Models for the southern San Andreas fault show dextral slip rates at the upper surface of the model that vary along the fault strands through the SGPr (Figure 3a and b).

In the Inactive Northern Pathway model (Figure 3a), the dextral slip rate along the San Bernardino strand (maroon) gradually decreases southward from Cajon Pass, with a small, stepped decrease in slip rate between Plunge Creek (site 3) and Wilson Creek (site A), where the San Gorgonio Pass thrust (green) takes up some dextral slip. Dextral slip rate along the San Gorgonio Pass thrust generally increases to the east to reach a maximum of 6 mm/yr dextral slip near its intersection with the Banning strand (coral). Because strike-slip is partitioned between both the San Gorgonio Pass thrust and a short active segment of the Banning strand that parallels the San Gorgonio Pass thrust (Figure 1), the dextral slip rate along the thrust varies along strike. The model produces a local low in dextral slip along the San Gorgonio Pass thrust at Millard Canyon (site 5). Dextral slip on the Garnet Hill strand (beige) decreases to the east, where the fault trace ends just short of reaching the Coachella segment of the San Andreas fault (brown). In contrast, dextral slip on both the Banning strand and the active portion of the Mission Creek strand (purple) increase to the east to maximum values where these faults merge with the Coachella segment.

In the Active Northern Pathway model (Figure 3b), the dextral slip rate along the San Bernardino strand decreases with distance from Cajon Pass, similar to slip rates of the Inactive Northern Pathway model (Figure 3a). However, unlike the Inactive Northern Pathway model, the dextral slip rate abruptly decreases between Badger Canyon (site 2) and Plunge Creek (site 3), due to the transfer of dextral slip onto the Mill Creek strand (blue). Farther to the east, dextral slip of ~10 mm/yr along the Mill Creek strand continues onto the Galena Peak strand (orange). The dextral slip rates along the Mission Creek and Banning strands gradually increase to the southeast where these strands merge with the Coachella segment.

Model reverse slip rates can be compared with recent reverse slip rates at Millard Canyon (site 5). The Inactive Northern Pathway model produces 3.5–6.2 mm/yr and the Active Northern Pathway model produces 3.6–4.5 mm/yr of reverse slip at Millard Canyon. The greater reverse slip of the Inactive Northern Pathway model is consistent with the greater strike-slip rate along the San Gorgonio Pass thrust along the southern slip pathway. Both reverse rates from the unconstrained models narrowly exceed the 1.8-3.5 mm/yr range determined by *Heermance and Yule* (2017) from offset alluvial terraces.

The Inactive Northern Pathway model matches more of the geologic strike-slip rates than the Active

Northern Pathway model (Figure 3a and b). Both unconstrained models underestimate strike-slip rates at Millard Canyon (site 5) on the San Gorgonio Pass thrust and overestimate slip rates at both Badger Canyon (site 2) and at Washington Street (site 7). While those are the only sites of slip rate mismatch for the Inactive Northern Pathway model, the Active Northern Pathway model also underestimates dextral slip rates at Burro Flats (site 4) and Painted Hills (site 6) and overestimates dextral slip rates at Three Palms (site 9). The Active Northern Pathway model has much greater dextral slip rate along the northern pathway and underestimates dextral slip rates at all sites along the southern slip pathway, except for Washington St. (site 7).

In the second pair of models, we constrain the slip rates at sites where rates from the unconstrained models lie outside of the geologic ranges. These applied slip rates use the limiting value at sites, which produces slip rate gradients adjacent to the applied slip rate regions (Figure 3c and d). The local slip rate gradients are not meant to represent local crustal conditions but reflect the incompatibility of the applied slip rate with the interpreted fault geometry. For both fault configurations (Figure 3c and d), the San Bernardino strand is pinned to the upper limit of the Badger Canyon slip rate (site 2), the San Gorgonio Pass thrust is pinned to the lower limit of the Millard Canyon dextral slip rate (site 5), and the Banning strand is pinned to the upper limit of the Washington Street slip rate (site 7). Additionally, the Active Northern Pathway model has pinned slip rates at the lower limits of the geologic slip rate range along the San Bernardino strand at Burro Flats (site 4) and along the Banning strand at Painted Hills (site 6). The Active Northern Pathway model slip rates are also pinned to the upper slip rate limit along the Mission Creek strand at Three Palms (site 9).

The Active Northern Pathway model has greater change in slip rate with the imposed constraints than the Inactive Northern Pathway model. Integrating the absolute value of change in slip rate along the San Andreas fault within this study area, the Active Northern Pathway model has 260 m^2/yr while the Inactive Northern Pathway has only 160 m^2/yr of slip rate change. Constraining the slip rates has the greatest impact on slip rate distribution where the greatest mismatch arises between the unconstrained model and the geologic estimates of slip rate. For example, the pinning of slip rates results in a slip rate distribution within the constrained models that differs significantly from both unconstrained models near Washington Street (site 7). The local reduction in slip rate produces sharp gradients in slip rate both east and west of the site in both the Inactive and Active Northern Pathway models. Local slip rate gradients also arise adjacent to other constrained sites. While the slip rate constraints in the Active Northern Pathway model locally impact slip, these constraints do not significantly alter the partitioning of slip between the northern and southern pathways. The Mission Creek strand maintains ~15 mm/yr of slip and the strands of the southern pathway maintain ~5 mm/yr of dextral slip.

The Active Northern Pathway model is not constrained at the Mission Creek alluvial complex (site B) within Figure 3b, even though some studies have found zero slip here along the Mission Creek fault strand (*Kendrick et al.*, 2015). Figure 4 provides an additional version of the constrained Active Northern Pathway model, which adds a constraint of zero dextral slip at the Mission Creek alluvial complex where slip rates are debated (site B). In similar manner as the other sites, constraining slip rate at the Mission Creek alluvial complex produces sharp local gradients in slip rate but does not shift the partitioning of slip rate between the two pathways.

3.5 Off-fault Deformation

To assess off-fault deformation within the fault system we sum the vorticity, which produces vertical axis rotation, and the dilation, which produces uplift/subsidence. This net off-fault deformation rate is calculated at distances greater than 1 km from active fault traces (Figure 5). Both models with unconstrained slip produce distributed off-fault deformation within both the western San Bernardino Mountains and the Little San Bernardino Mountains (Figure 5a and b). In the unconstrained models of both fault configurations, localized off-fault deformation develops near many fault intersections and geometric irregularities where strike-slip is hindered by these irregularities. Within the Active Northern Pathway model, the irregularities along the southern slip pathway produce lesser local off-fault deformation because the southern pathway has lesser dextral slip rate than the Inactive Northern Pathway model (Figure 4; *Beyer et al.*, 2018).

The Inactive Northern Pathway model produces greater off-fault deformation in the southern San Bernardino Mountains than the Active Northern Pathway model. Slip along the additional active fault strands of the northern pathway reduces the local off-fault deformation. Consequently, the mean off-fault deformation calculated > 1 km from active faults in the study area decreases with the addition of the northern slip pathway. The slightly lower mean off-fault deformation of the Active Northern Pathway model (83 nanostrain/yr) compared to the Inactive Northern Pathway model (87 nanostrain/yr) is consistent with the findings that adding more faults to the system generally allows for greater fault slip and less off-fault deformation (*Madden et al.*, 2017; *McBeck et al.*, 2017).

The uplift pattern for both models shows uplift within the San Bernardino mountains. Because the fault geometry used here differs slightly from the models used by *Fattaruso et al.* (2016), the uplift is very close to that produced in the 2016 study. Updates include the dip of the Garnet Hill and Banning strands and the activity along the Galena Peak strand. *Fat-*

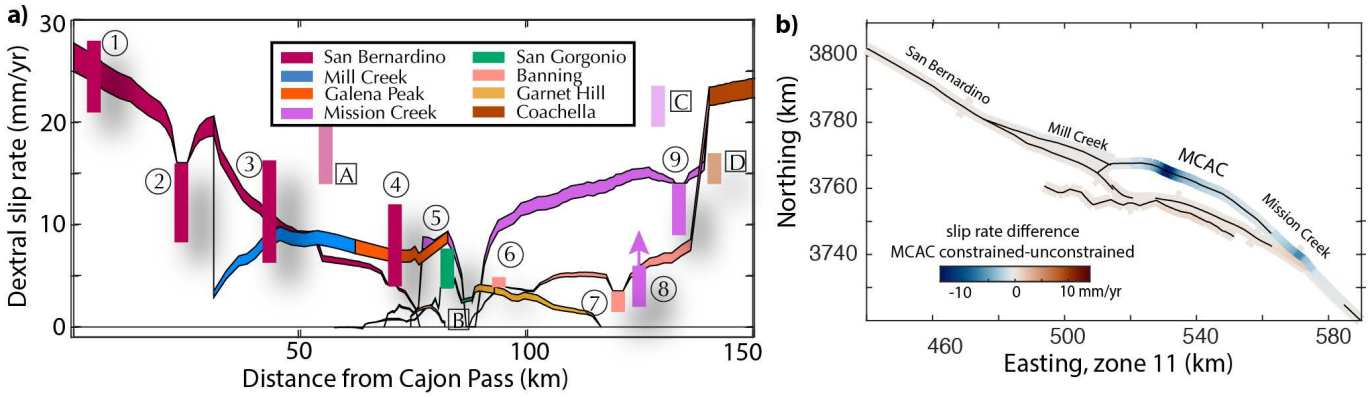

Figure 4 – a) Dextral slip rates along strands of San Andreas fault at the upper surface of the model for the constrained Active Northern Pathway model of Figure 3d that also limits slip rate to zero at the Mission Creek alluvial complex (MCAC). Vertical bars show the geologic slip rates at sites labeled in Figure 11 - lighter hued bars are slip rates that are not used for the model assessment. **b)** Difference in slip rate between the constrained Active Northern Pathway model of Figure 3d and the model with MCAC also constrained to have zero slip.

taruso et al. (2016) show that time averaged uplift over the past 1 Ma that considers changes to active fault geometry matches rock exhumation patterns. In addition to uplift in regions of net off-fault deformation, dip slip on faults contributes to the uplift pattern. Both models show subsidence in the San Bernardino basin that is consistent with geodetic measurements (*Wisely and Schmidt*, 2010). The results highlight several regions where recent uplift data might distinguish between the two plausible models (roman numerals on Figure 5e and f). The Inactive Northern Pathway model predicts greater subsidence at the Banning bench (site i) than the Active Northern Pathway. At site ii, east of the Mission Creek Alluvial Complex, the Inactive Northern Pathway model predicts uplift while the Active Northern Pathway model predicts subsidence. The modeled uplift patterns reflect vertical movement over many earthquake cycles, Consequently, geomorphic data, such as exposure ages from recent alluvial deposits, in these regions may provide valuable constraints to distinguish between the two models.

3.6 Influence of Slip Rate Sites on each Other

We assess the influence of slip rates at each site on other sites with a suite of models that apply 1 mm/yr of dextral slip at each slip rate site independently. The tables of Figure 6b and c show the resulting dextral slip rate detected at each site due to 1 mm/yr dextral slip applied to the sites listed in the first column of the table. Because the Mission Creek alluvial complex (site B) is not part of the Inactive Northern Pathway model, it does not have any impact within that model.

The influence of sites varies within the system, and nearby sites have greater influence on each other than distal sites. For example, within both the Inactive and Active Northern Pathway models, the cluster of sites within the Indio Hills (sites 7-9, C and D) have a large influence on each other (Influence Factor 0.2–0.5; Figure 6b and c). The influence tables are slightly asymmetric indicating that the influence of slip at one site on another site is not necessarily reciprocal. For example, in the Active Northern Pathway model, 1 mm/yr at the Plunge Creek (site 3) produces only 0.06 mm/yr at Badger Canyon (site 2) while 1 mm/yr at Badger Canyon produces 0.10 mm/yr at Plunge Creek. In other words, changes in slip at Badger Canyon have greater influence at Plunge Creek than vice versa in this model. The site influences between the Badger Canyon and Plunge Creek sites are more symmetric in the Inactive Northern Pathway model, which suggests that the presence of the fault branch between Badger Canyon and Plunge Creek in the Active Northern Pathway model, reduces the influence of dextral slip at Plunge creek on Badger Canyon. The additional active northern strand also changes the influence of the Wilson Creek (site A) between the Active and Inactive Northern Pathway models. Most other sites have similar influences on each other between the two models.

The influence of sites on each other generally decreases with distance between sites (Figure 6d). The best fitting exponential curve through the results shows decreasing influence with distance for sites within 20 km of each other. In addition to this trend, some sites within 5–20 km of each other have anomalously low and high influence. Three pairs of sites with relatively low influence (1- Burro Flats & Millard Canyon; 2- Mission Creek alluvial complex & Painted Hills; 3- Washington Street & Thousand Palms) are highlighted in blue on Figures 6a and 6d while three pairs of sites with relatively high influence (1- Cajon Creek & Badger Canyon; 2- Plunge Creek & Wilson Creek; 3- Thousand Palms & Three Palms) are highlighted in red on Figures 6a and 6d. For example, the Badger Canyon and Cajon Creek sites have similar distance (19 km) as the Burro Flats and Painted Hills sites (19 km) but have much larger influence on each other (~0.12 > 0.01). The three pairs of low influence sites for their distances all occur on different segments or parallel branches of the fault system. Even though the sites are nearby one another,

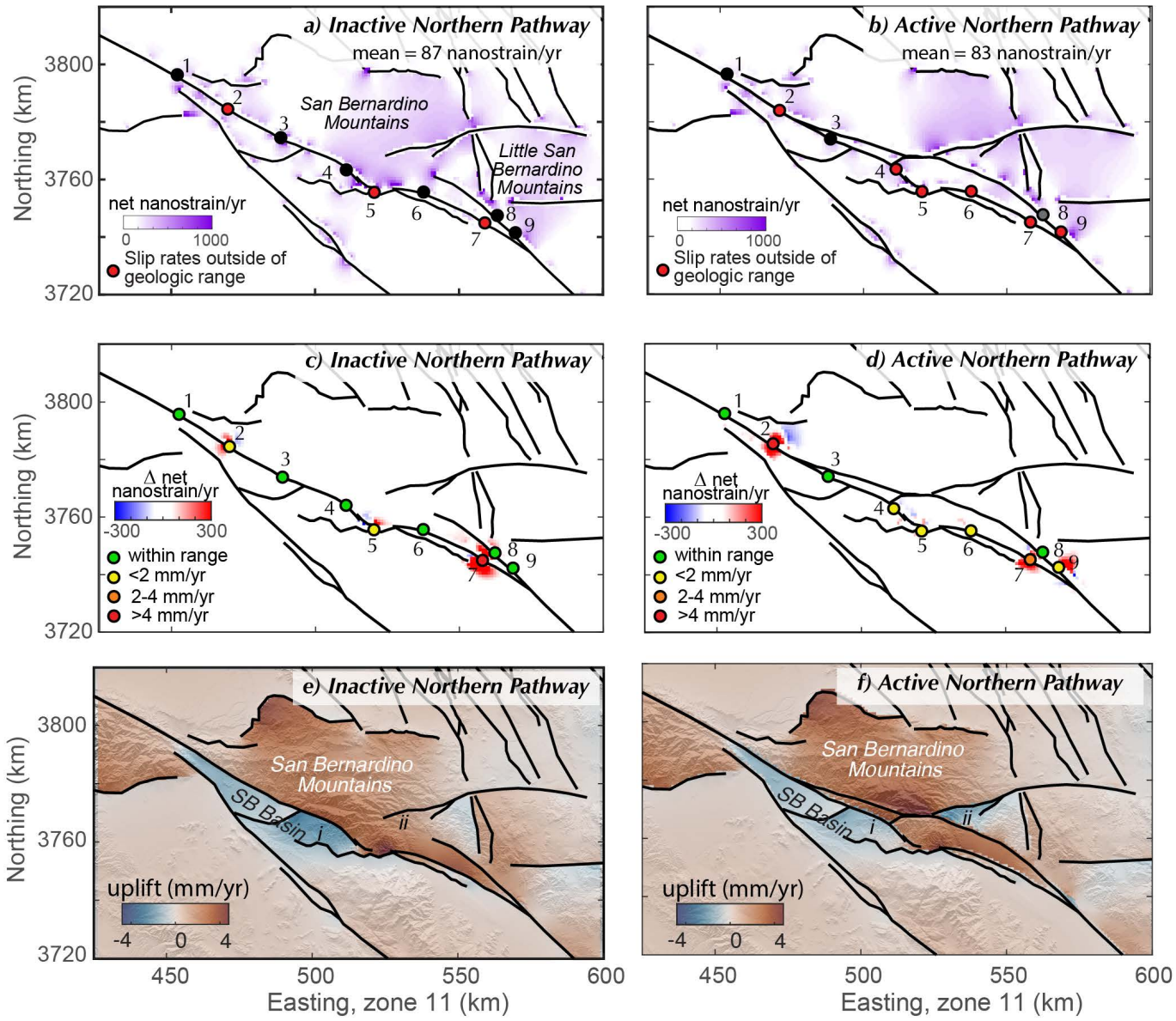

Figure 5 – Net off-fault strain maps from Inactive Northern Pathway **(a and c)** and Active Northern Pathway (**(b and d)** models, each with tectonic loading at midpoint of the applied range. The top row **(a and b)** shows strain for the unconstrained models. The middle row **(c and d)** shows the difference between the unconstrained and the models where slip rates are not permitted to exceed the geologic ranges (constrained-unconstrained). Red indicates regions of increased off-fault deformation when slip rates are constrained for that fault system configuration. The bottom row **(e and f)** shows the uplift rate pattern, which is due to a combination of off-fault deformation and dip-slip along faults. SB Basin: San Bernardino Basin.

slip at one does not influence slip on the nearby site because of the lack of fault connectivity at these distances. Pairs of sites on branched faults that are situated very close to the branch, such as Washington Street and Thousand Palms, have influence consistent with the general trend on Figure 6d because slip at one of these sites is close enough to where the faults intersect that slip on one branch can influence the nearby branch. The pairs of sites that have relatively high influence for their distances all occur along continuous portions of the fault without branches, segments, or kinks. Dextral slip transmits more easily along the continuous segments so that slip at one site has a high influence on other sites along the continuous segment.

3.7 Impact of each Slip Rate Site on the Fault System

While Figure 6 shows how each site influences slip rate at other sites, that analysis does not inform the impact of the sites' slip rates on the stretches of fault between the sites. To assess this, we map the dextral slip in response to the applied 1 mm/yr at each site and integrate the slip along the faults to derive the total impact factor (Figure 7). The piecewise integration excludes the patch with applied slip rate and also excludes sections of the faults with less than 2% of the applied slip rate (slip < 0.02 mm/yr). In this study, we only prescribe slip rate for the upper 2 km of the fault surface – deeper portions of the faults are free to slip. If these patches of applied slip rate were extended to greater depths, we would see greater values for the

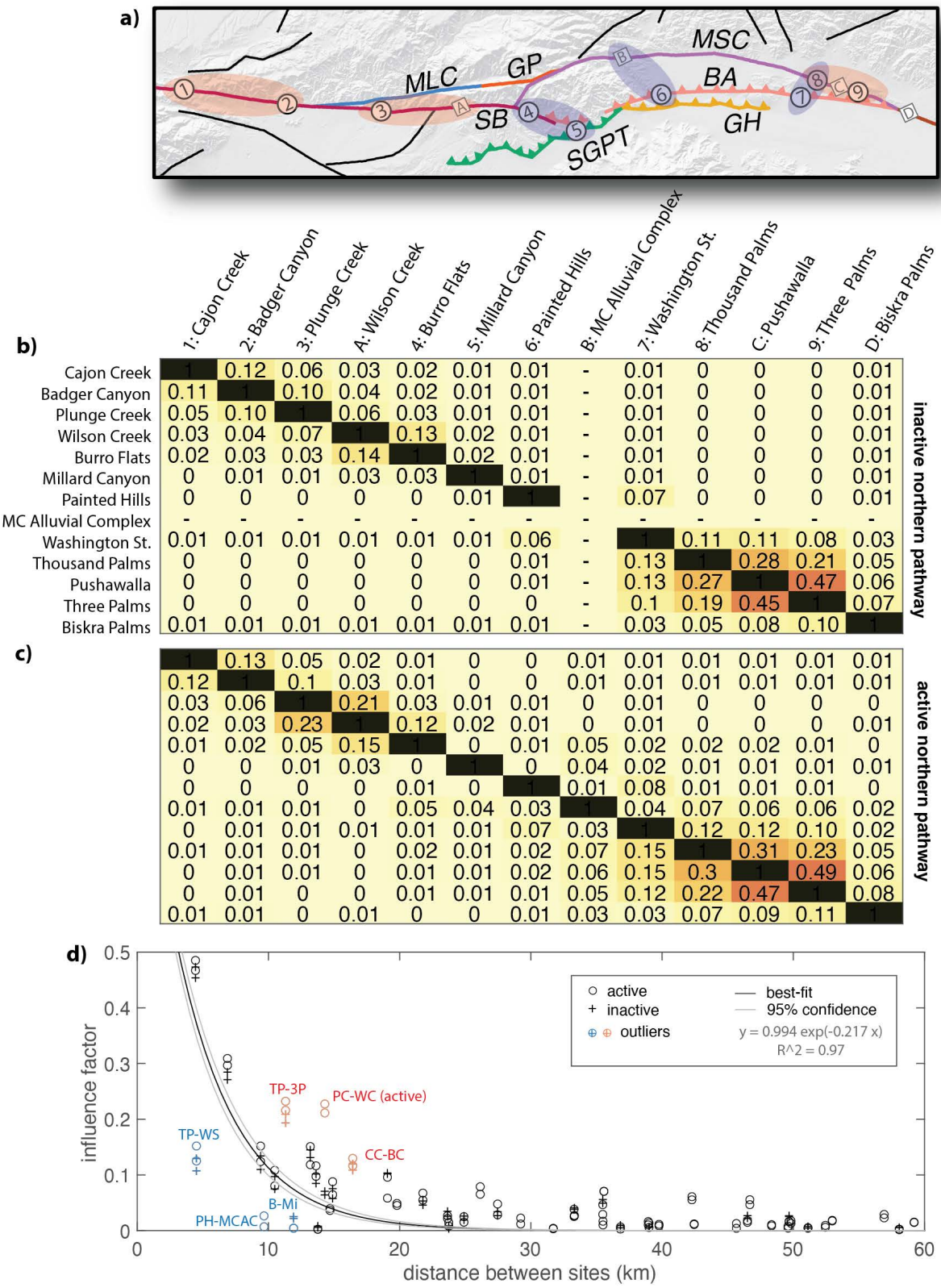

Figure 6 – Influence of 1 mm/yr dextral slip applied at sites listed at left on all other sites in the model. **a)** Map of the site locations with ellipses highlighting pairs of sites with relative high influence (red) and low influence (blue). **b)** and **c)** influence for Inactive Northern Pathway and Active Northern Pathway models respectively. The diagonals of the table are all 1%, reflecting the influence of each site on itself while the off-diagonals show influence values less than one. **d)** Correlation of influence factor with distance between sites shows that nearby sites have greater influence on each other than distal sites. Lines show an exponential best fit to all the data. Outliers to the best fit are highlighted in red and blue. TP: Thousand Palms; 3P: Three Palms; PC: Plunge Creek; WC: Wilson Creek; CC: Cajon Creek; BC: Badger Canyon; WS: Washington Street; PH: Painted Hills; MCAC: Mission Creek Alluvial Complex; B: Burro Flats; Mi: Millard Canyon. MLC: Mill Creek; GP: Galena Peak; SGPT: San Gorgonio Pass Thrust; GH: Garnet Hill; BA: Banning; MSC: Mission Creek.

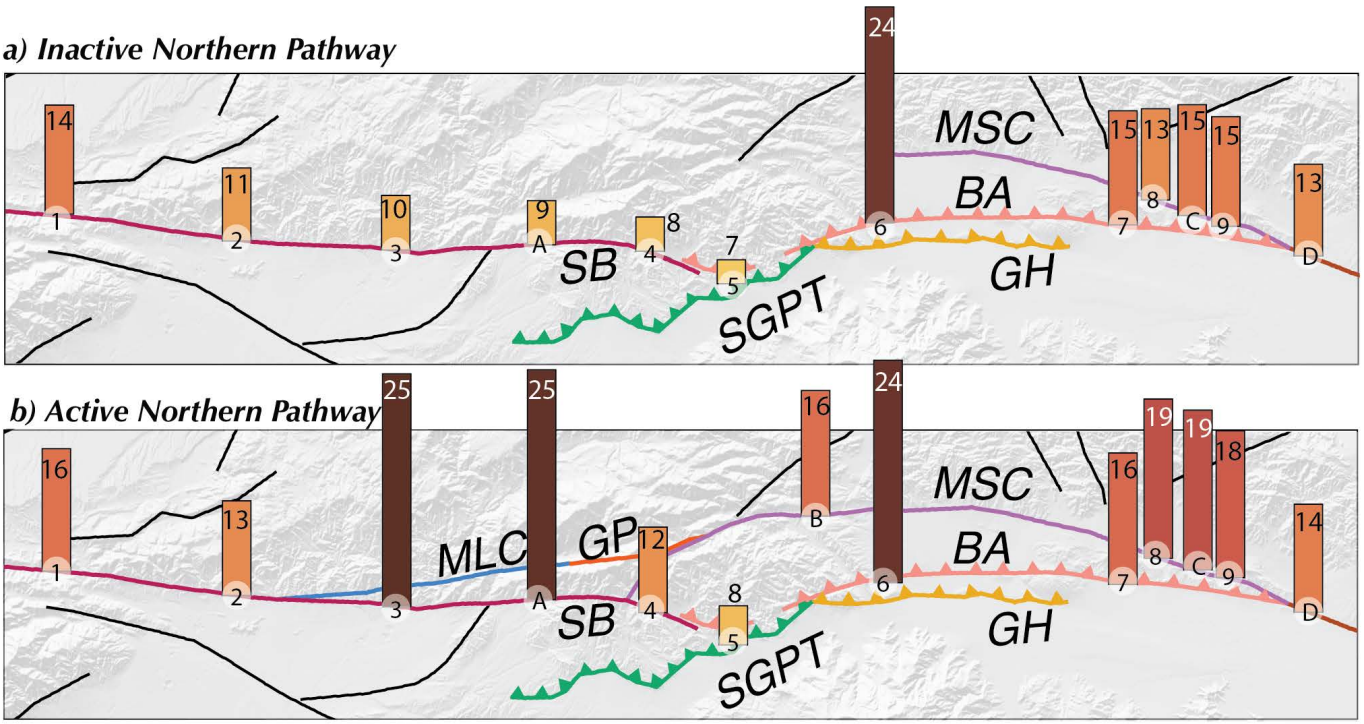

Figure 7 – Slip rate impact factors for both the **a)** Inactive Northern Pathway and **b)** Active Northern Pathway models. The darkness and height of the bar represent the impact factor value of each site. MLC: Mill Creek; GP: Galena Peak; SGPT: San Gorgonio Pass Thrust; GH: Garnet Hill; BA: Banning; MSC: Mission Creek.

impact factors among sites and on the system, but the relative impact may be similar.

The Inactive and Active Northern Pathway models show similar patterns of slip rate impact factor for most sites (Figure 7). The impact factors of the sites range from 7 to 25. The lowest impact factor (IF) is at the Millard Canyon site for both model geometries. Sites along the San Bernardino strand in the Inactive Northern Pathway model also have relatively low impact factors. The application of 1 mm/yr of slip rate at these sites produces less slip rate along the fault system than applied slip rate at the other sites, implying that applied slip rate along the San Bernardino strand produces greater off-fault deformation in the Inactive Northern Pathway model. For Millard Canyon, off-fault deformation may arise because the site is located within a segmented portion of the southern San Andreas fault, along the San Gorgonio Pass thrust, which does not at the surface meet with the San Bernardino strand. This segmentation leads to greater off-fault deformation in this region.

The Painted Hills (site 6), which has low influence on other sites (Figure 6) has the greatest impact factor of the sites in the Inactive Northern Pathway model (Figure 7). Because this site sits on the Banning strand, which merges with the parallel-striking Garnet Hill strand at depth, slip rates imposed on the Banning strand also impact slip rates on the Garnet Hill strand. The slip distributions plotted on Figure 8 show how slip rate applied at Painted Hills impacts nearby fault strands. The Garnet Hill strand doesn't yet have any slip rate sites, so the interaction of the Banning and Garnet Hill strands was not considered in the site analysis of Figure 6. The Washington Street (site 7) also occurs along the Banning strand but has a lower impact factor than the Painted Hills site because the Garnet Hill strand is not active as far east as site 7. Furthermore, while the Banning strand merges at depth to the Mission Creek strand at the Washington Street site, these two faults meet much deeper than the Garnet Hill and Banning faults (Figure 1). Consequently, the transmission of surface slip rates from the Banning to Mission creek strands at Washington Street is not as effective as the transmission of slip rates from the Banning to Garnet Hills strands at the Painted Hills site.

Due to the longer active fault trace in the Active Northern Pathway model, slip from the Washington Street site as well as slip from sites along the Mission Creek strand and Coachella segment extends much farther northwest along the Mission Creek strand than in the Inactive Northern Pathway model (Figure 8). This increase in slip extent with the Active Northern Pathway model also increases the impact factor of all of the sites.

While most sites increase their impact by 1–3 with the addition of the northern pathway to host dextral slip, the Mission Creek Alluvial Complex and the Plunge Creek and Wilson Creek sites along the San Bernardino strand have impact increases of 15–16. The impact increase for the Mission Creek Alluvial Complex reflects that this site has zero slip within the Inactive Northern Pathway model. For the Plunge Creek and Wilson Creek sites, the close branch angle between the San Bernardino and Mill Creek strands (~10°) allows dextral slip applied along one branch to

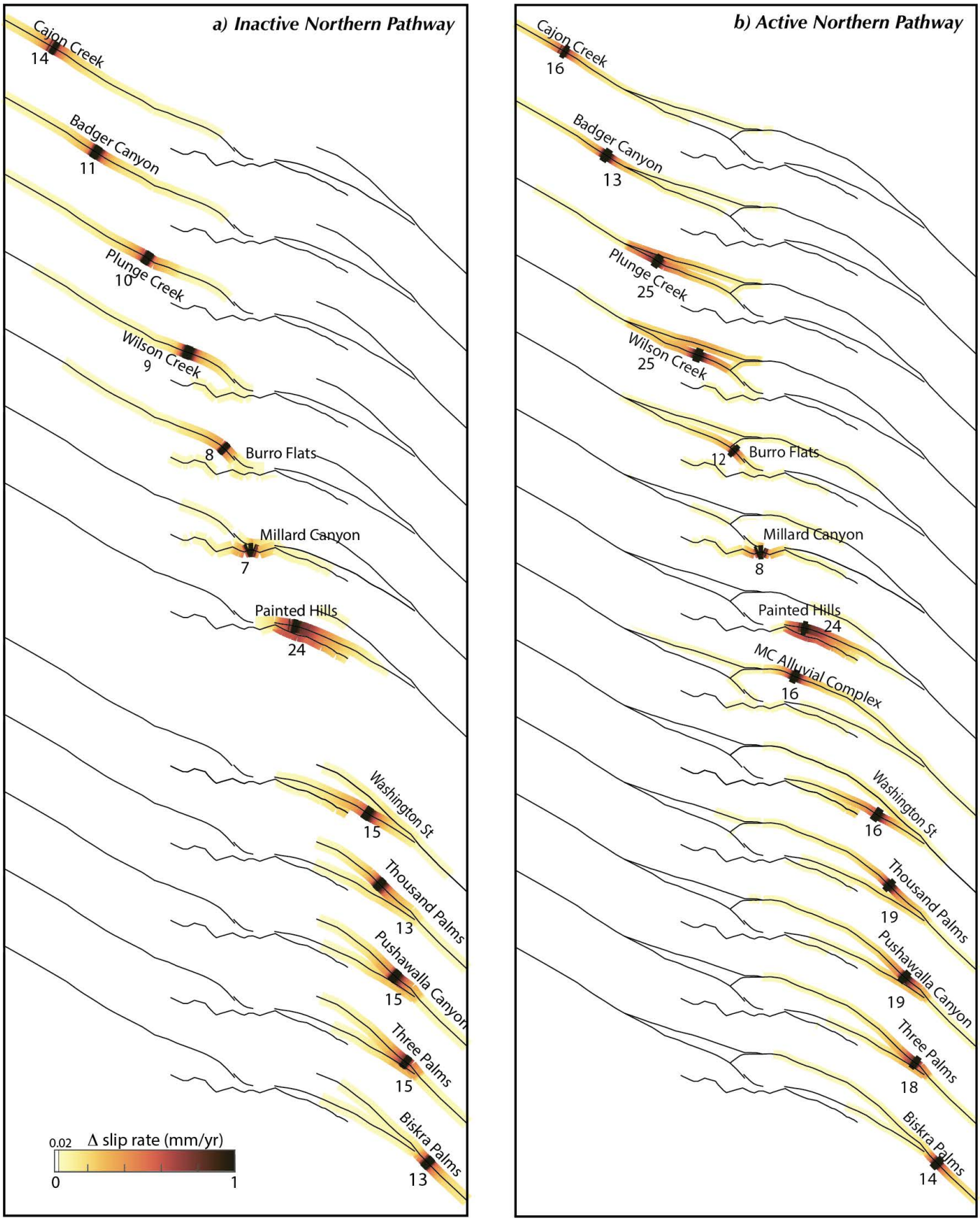

Figure 8 – Distribution of dextral slip rate in response to applied slip at each site within the **a)** Inactive Northern Pathway and **b)** Active Northern Pathway models. On slip rates greater than 2% of applied rate are plotted. Numbers report the integrated impact factor along the faults (IF in m^2/yr).

produce shear tractions on the other branch that increase the impact factor compared to the model without the branch. Because these sites are within a fault branch in the Active Northern Pathway model, they have high impact factor like the Painted Hills site.

The impact factor of sites along branches is greater

than the impact factor of sites that lie outside merge of the two branches. For example, in the Active Northern Pathway model, the impact factor of the Plunge Creek and Wilson Creek sites is greater than that of the Badger Canyon site, north of the branch of the San Bernardino strand with the Mill Creek Strand. The applied slip rate at sites along one branch impacts the other branch much more than applied slip rate at sites outside the merge of the two fault branches. Also in both models, sites along the Mission Creek and Banning strands have greater impact factors than the Biskra Palms site, which is located south of the merger of the Banning and Mission Creek strands.

4 Discussion

Slip rate uncertainties typically derive from the interpretation of offset units (e.g., *Cowgill*, 2007), offset measurements (e.g., *Gold et al.*, 2009) and the age of materials (e.g., *Prush and Oskin*, 2020). Studies also show that slip rates can vary over tens of thousands of years (e.g., *Rittase et al.*, 2014; *Hatem et al.*, 2020; *Elston et al.*, 2022; *Zinke et al.*, 2017), which makes older rates less reliable estimates of current activity. The uncertainties of slip rate estimates can be large enough to permit a variety of active fault geometry interpretations. For example, the Inactive and Active Northern Pathway models predict dextral slip rates that differ by ~5 mm/yr at Plunge Creek (site #3; Figure 3) south of where the northern and southern pathways branch; however, both model predictions fall within the slip rate uncertainty of *McGill et al.* (2013). In the face of these large uncertainties, collecting slip rate data from additional sites provides one way to constrain active slip partitioning but the results of this study demonstrate that not all sites provide the same impact on our understanding of the active fault system deformation.

4.1 High and Low Impact Structural Positions along the Fault System

Within fault systems that have multiple intersecting active faults, the impact factor of sites depends on their position within the fault system. This dependence of slip rate on structural position means that even sites close to each other may have very different impact on the deformation of the fault system (Figure 7). Sites along parallel or subparallel branched fault segments, such as the Painted Hills and Plunge Creek sites in the Active Northern Pathway model, have greater impact on the fault system than sites outside of the branch because slip is transmitted between connected parallel fault segments. At the same time sites along unconnected strands or near intersecting faults that are not parallel or subparallel, such as the Burro Flats and Millard Canyon sites, have low impact factor.

The geologic slip rates typically have uncertainties much larger than the 1 mm/yr applied to the slip rate sites in the assessment of the sites' impact. Consequently, changes of slip rate within the range of slip rate uncertainty at some sites of geologic slip rate investigation can have a large impact on the partitioning of deformation within the fault system. Along planar strike-slip faults, different sites may have similar impact on the system; however, sites along the San Andreas fault through the San Gorgonio Pass region, which geometry is more complex, produce significantly different slip rate impacts with structural position. Slip rate sites along fault branches necessitate detailed consideration because these areas have high impact factors, as slip on one branch impacts slip along the other.

Sites along irregular or disconnected faults have low impact factors and greater nearby off-fault deformation. For example, the Burro Flats and Millard Canyon sites are along relatively disconnected fault strands so that they have both low influence on other sites (Figure 6) and low impact on the nearby fault system (Figures 7 and 8). The irregular geometry of the San Gorgonio Pass thrust and its connection to the southern end of the San Bernardino strand impedes transmission of dextral slip along the southern slip pathway and contributes to off-fault deformation (Figure 5). The local accumulation of off-fault deformation may promote distributed inelastic deformation, such as via pressure solution creep (e.g., *Gratier et al.*, 1999) or cleavage development (e.g., *Elliott et al.*, 1976).

4.2 Incompatibility of Slip Rates and Fault Geometry

Where the mechanical model produces slip rates that are consistent with the geologic observations, we confirm that the tested fault geometry is mechanically and kinematically compatible with the estimated slip rates. However, regions where slip rates from the numerical model do not agree with geologic estimates may have incompatibility between the tested fault geometry and slip rate and produce off-fault deformation. In the models with constrained slip rates, this off-fault deformation increases (Figure 5c and d). For both the unconstrained and the constrained models, the Active Northern Pathway model produces lesser off-fault deformation than the Inactive Northern Pathway model because the addition of the Mill Creek strand provides an additional opportunity for accommodation of strain as fault slip rather than off-fault deformation.

Little to no change in off-fault deformation occurs where the unconstrained model fault slip rates are within or near the limits of the geologic ranges. The compatibility of dextral slip rates with interpreted fault geometry doesn't preclude the possibility that the models inaccurately represent the subsurface fault configuration. For example, geophysical evidence suggests that rather than the vertical dip represented in this study, the San Bernardino strand may dip to the northeast *Fuis et al.* (2012). Both verti-

cal and dipping faults can accommodate strike slip so that variations in fault dip might not produce distinguishable dextral slip rates (e.g., *Fattaruso et al.*, 2014).

Regions with mismatched slip rates in both the Inactive and Active Northern Pathway models (Figure 3), Washington Street (site 7) and Badger Canyon (site 2), indicate that slip rates in these regions may be kinematically incompatible with the interpreted active fault geometry near these sites. These incompatibilities highlight the need for additional constraints on subsurface active fault configuration in these regions. While microseismicity during the interseismic period can illuminate subsurface active fault geometry, such as along the San Jacinto fault (*Ross et al.*, 2017), the southern San Andreas fault has not produced much microseismicity during the recorded catalog. Uncertainty persists on the subsurface geometry of active faults in these regions. For example, at Cajon Pass, the San Andreas and San Jacinto faults may be connected at depth even though the surface traces are separated by several km (e.g., *Matti and Morton*, 1993; *McGill et al.*, 2013). A hard connection at depth between these faults would alter slip distribution among the faults. Mechanical models of *Herbert et al.* (2014) show that connecting the San Jacinto and San Andreas faults reduces dextral slip rates at the Badger Canyon (site 2), which would better match the site's geologic slip rates.

Near the Indio Hills, the Banning and Mission Creek strands merge into the Coachella segment of the San Andreas fault. The subsurface geometry of the faults near this intersection is not well constrained (e.g., *Fuis et al.*, 2017). The off-fault deformation in this region and the mismatch to geologic slip estimates (Figure 5) could be a result of incorrectly inferred fault geometry. For example, while the Garnet Hill strand does not produce surface expression of active faulting, it may connect to the Coachella segment at depth. If the models included such a connection, the Garnet Hill strand might take up dextral slip rate currently partitioned to the Banning strand.

4.3 Potential Data to Assess Activity along Northern Slip Pathway

The results of this study and that of *Beyer et al.* (2018) show that adding a northern pathway for fault slip modifies slip distribution. While the Mission Creek strand shows evidence of recent slip near its intersection with the Banning strand, debate persists on the activity of the northern slip pathway near and northwest of the Mission Creek alluvial complex (*Beyer et al.*, 2018; *Fosdick and Blisniuk*, 2018; *Kendrick et al.*, 2015). This study is not able to ascertain between the two viable models, but it does highlight areas where additional geologic data may provide critical evidence for the partitioning of slip along faults. Because the northern slip pathway was active > 100 ka, we need young ages along the northern pathway to resolve current activity (*Kendrick et al.*, 2015). Furthermore, the region's complex history provides several potential slip surfaces so that low slip rate along one fault does not preclude another nearby fault accommodating dextral slip along a northern pathway. Nevertheless, we can benefit from additional slip rates from the various faults along the northern pathway, such as the Galena Peak and Mill Creek strands.

Slip along the northern pathway also impacts deformation in the region that can be used to delineate between the plausible active fault models. The Wilson Creek site (#4) has slip rates that differ by 5 mm/yr between the Inactive and Active Northern Pathway models. Because the age of the alluvial fan was estimated from soil chronology (*Harden and Matti*, 1989) rather than modern dating techniques, redating of this surface might provide substantial improvement to our understanding of strain partitioning and potential activity of the northern pathway. Additionally, uplift rates from the region between the Pinto Mountain fault and the Mission Creek strand (region labeled ii on Figure 5) could distinguish between the models. In this region, the model predicts uplift if the northern pathway is inactive and subsidence if the norther pathway is active. Such additional geologic data would be valuable for resolving the ongoing debate about activity along the northern strand of the San Andreas fault.

The two alternative models also predict differing degrees of off-fault deformation between the southern and northern pathways (Figure 5); the Active Northern Pathway produces negligible off-fault deformation between the pathways while the Inactive Northern Pathway model produces ~500 nanostrain/yr. However, documenting recent off-fault deformation rates can be challenging. The catalog of microseismicity in this region may indicate significant secondary deformation (e.g, slip along existing surfaces), but this deformation may vary through the earthquake cycle and might not represent long-term strain partitioning. Furthermore, the lack of microseismicity does not confirm lack of strain accumulation. Current off-fault deformation rates are difficult to constrain with geologic data. Most methods of estimating off-fault deformation rates, such as paleomagnetic records of vertical axis rotation (e.g., *Titus et al.*, 2011) and folding of contracted units (e.g., *Scharer et al.*, 2004), are generally not available for young unlithified sediments. Data collected from units older than 100 ka need to consider the variation in fault activity in the region (*Fattaruso et al.*, 2016), which complicates the delineation of current fault activity.

4.4 Seismic Hazard

The numerical models demonstrate the high spatial variability of strike-slip rates along faults with nonplanar configuration. The well-studied southern San Andreas fault investigated here has far more slip rate sites than most strike-slip fault systems with restraining bends and branches. In this study, the model re-

sults confirm the estimated slip rates that range from 5 to 25 mm/yr along the southern San Andreas faut. In other regions of complex faulting that lack sufficient slip rate estimates to reveal spatial variations, numerical models can inform slip rate distribution and strengthen seismic hazard assessments.

Numerical models can also highlight regions where additional data could shed significant insight on regional deformation. This study demonstrates that strike-slip fault branches show particularly high spatial variability of slip rate (Figure 3), accrual of nearby off-fault deformation (Figure 5) and impact on the fault system (Figures 7 and 8). Fault branches warrant detailed investigation in order to understand regional strain partitioning. Furthermore, the range of impact factors for the different sites demonstrates that not all slip rate sites have equal impact on the fault system. Consequently, if we have errors or are off in our estimate of slip rate at any one of the more sensitive sites, such as those at fault branches, this error may have a large impact on our understanding of the deformation of the fault system and thus hinder our ability to accurately assess seismic hazard in the region.

5 Conclusions

We use three-dimensional numerical crustal deformation models to analyze the role of slip rate sites in determining deformation of the southern San Andreas fault system within the San Gorgonio Pass region. We investigate the compatibility of models with and without active slip along the northern pathway of the San Andreas fault around the San Gorgonio Pass region with geologic slip rates. Within unconstrained models that allow all faults to slip freely everywhere in response to tectonic loading and fault interaction, the Active Northern Pathway model produces slip rates with greater mismatch to young (< 40 ka) slip rate estimates at sites of geologic investigations than the Inactive Northern Pathway model. To assess incompatibilities between fault geometry and slip rate, we utilize a new approach and constrain the slip rates along the faults to within the geologic range at each geologic slip rate site. Slip rate adjustments in the constrained model ensure that the model matches all geologic slip rates, but this produces local off-fault deformation near the constrained sites.

Maps of off-fault deformation show that the Inactive Northern Pathway fault configuration for both the unconstrained and the constrained models has greater off-fault deformation than the Active Northern Pathway. The additional northern slip pathway provides an opportunity for a greater amount of deformation to be expressed as fault slip. While fault systems may evolve to reach more efficient configurations (e.g., *Hatem et al.*, 2017; *McBeck et al.*, 2017), this does not mean that the presently active configuration must be the most optimal. Additional slip rate constraints and data off-fault deformation rates within the southern San Andreas system would provide valuable information to assess between the two alternative configurations.

We assess how much of an impact the incompatibilities between fault geometry and geologic slip rate have on the system by assessing the impact of slip rate changes. Small changes of slip rate at any one site of geologic slip rate investigation impact slip rates elsewhere in the system. However, this impact is not the same for all sites, which means that inaccuracies in the slip rate that we use for seismic hazard analysis may have differing impact along active fault systems at one site than another. The degree of impact that slip rate sites have on the fault system depends on their structural positions. Sites along segmented faults may have lesser impact than sites along a continuous fault segment, and sites along fault branches have the greatest impact. Fault branches along strike-slip faults require detailed investigation because these areas have high spatial variability of slip rate and can impact the nearby branches of the fault system, adding additional uncertainty to our current assessment of the seismic hazard.

Acknowledgements

This research was partially supported by the Southern California Earthquake Center (Contribution No. 11878). SCEC is funded by NSF Cooperative Agreement EAR-1600087 & USGS Cooperative Agreement G17AC00047. The authors thank two anonymous reviewers of a previous version of this manuscript as well as Rebecca Bell, Sam Wimpenny and Craig Magee for reviewing this manuscript.

Author contributions

Conceptualization: J. Hatch, M. Cooke.
Formal Analysis: J. Hatch, M Cooke, H. Elston.
Writing – original draft: J. Hatch, M. Cooke.
Writing – review and editing: M. Cooke, J. Hatch, H. Elston.

Data availability

The crustal deformation software Poly3D is made available by the Stanford Tectonic Geomorphology lab at https://github.com/stgl/poly3d. Input files for the unconstrained and constrained Active Northern Pathway and Inactive Northern Pathway models used in this study can be downloaded from (dx.doi.org/10.6084/m9.figshare.20274363).

Competing interests

The authors declare no competing interests.

Peer review

This publication was peer-reviewed by Rebecca Bell and Sam Wimpenny. The full peer-review report can be found here: https://tektonika.online/index.php/home/article/view/38/21

Copyright notice

References

Becker, T. W., J. L. Hardebeck, and G. Anderson (2005), Constraints on fault slip rates of the southern California plate boundary from GPS velocity and stress inversions, *Geophysical Journal International*, *160*(2), 634–650, doi: 10.1111/j.1365-246X.2004.02528.x.

Behr, W. M., D. H. Rood, K. E. Fletcher, N. Guzman, R. Finkel, T. C. Hanks, K. W. Hudnut, K. J. Kendrick, J. P. Platt, W. D. Sharp, R. J. Weldon, and J. D. Yule (2010), Uncertainties in slip-rate estimates for the Mission Creek strand of the southern San Andreas fault at Biskra Palms Oasis, southern California, *GSA Bulletin*, *122*(9-10), 1360–1377, doi: 10.1130/B30020.1.

Beyer, J., M. L. Cooke, and S. T. Marshall (2018), Sensitivity of deformation to activity along the Mill Creek and Mission Creek strands of the southern San Andreas fault, *Geosphere*, *14*(6), 2296–2310, doi: 10.1130/GES01666.1.

Blisniuk, K., K. Scharer, W. D. Sharp, R. Burgmann, C. Amos, and M. Rymer (2021), A revised position for the primary strand of the Pleistocene-Holocene San Andreas fault in southern California, *Science advances*, *7*(13), doi: 10.1126/sciadv.aaz5691.

Comninou, M., and J. Dundurs (1975), The angular dislocation in a half space, *Journal Of Elasticity*, *5*(3-4), 203–216, doi: 10.1007/bf00126985.

Cooke, M. L., and L. C. Dair (2011), Simulating the recent evolution of the southern big bend of the San Andreas fault, Southern California, *Journal of geophysical research*, *116*(B4), doi: 10.1029/2010jb007835.

Cooke, M. L., M. T. Schottenfeld, and S. W. Buchanan (2013), Evolution of fault efficiency at restraining bends within wet kaolin analog experiments, *Journal of Structural Geology*, *51*, 180–192, doi: 10.1016/j.jsg.2013.01.010.

Cooke, M. L., K. Toeneboehn, and J. L. Hatch (2020), Onset of slip partitioning under oblique convergence within scaled physical experiments, *Geosphere*, *16*(3), 875–889, doi: 10.1130/GES02179.1.

Cowgill, E. (2007), Impact of riser reconstructions on estimation of secular variation in rates of strike–slip faulting: Revisiting the Cherchen River site along the Altyn Tagh Fault, NW China, *Earth and planetary science letters*, *254*(3), 239–255, doi: 10.1016/j.epsl.2006.09.015.

Crider, J. G., and D. D. Pollard (1998), Fault linkage: Three-dimensional mechanical interaction between echelon normal faults, *Journal of geophysical research*, *103*(B10), 24,373–24,391, doi: 10.1029/98jb01353.

Dawers, N. H., and M. H. Anders (1995), Displacement-length scaling and fault linkage, *Journal of Structural Geology*, *17*(5), 607–614, doi: 10.1016/0191-8141(94)00091-D.

DeMets, C., R. G. Gordon, and D. F. Argus (2010), Geologically current plate motions, *Geophysical Journal International*, *181*(1), 1–80, doi: 10.1111/j.1365-246X.2009.04491.x.

Di Toro, G., T. Hirose, S. Nielsen, G. Pennacchioni, and T. Shimamoto (2006), Natural and experimental evidence of melt lubrication of faults during earthquakes, *Science*, *311*(5761), 647–649, doi: 10.1126/science.1121012.

Dibblee, T. W. (1964), Geologic map of the San Gorgonio Mountain quadrangle, San Bernardino and Riverside Counties, California, *Tech. Rep. I-431*, US Geological Survey.

Elliott, D., J. G. Ramsay, and D. S. Wood (1976), A discussion on natural strain and geological structure - the energy balance and deformation mechanisms of thrust sheets, *Philosophical transactions of the Royal Society of London. Series A: Mathematical and physical sciences*, *283*(1312), 289–312, doi: 10.1098/rsta.1976.0086.

Elston, H., M. Cooke, and A. Hatem (2022), Non-steady-state slip rates emerge along evolving restraining bends under constant loading, *Geology*, *50*(5), 532–536, doi: 10.1130/G49745.1.

Fattaruso, L. A., M. L. Cooke, and R. J. Dorsey (2014), Sensitivity of uplift patterns to dip of the San Andreas fault in the Coachella Valley, California, *Geosphere*, *10*(6), 1235–1246, doi: 10.1130/GES01050.1.

Fattaruso, L. A., M. L. Cooke, R. J. Dorsey, and B. A. Housen (2016), Response of deformation patterns to reorganization of the southern San Andreas fault system since ca. 1.5Ma, *Tectonophysics*, *693*, 474–488, doi: 10.1016/j.tecto.2016.05.035.

Fay, N. P., and E. D. Humphreys (2005), Fault slip rates, effects of elastic heterogeneity on geodetic data, and the strength of the lower crust in the Salton Trough region, southern California, *Journal of Geophysical Research, [Solid Earth]*, *110*(B9), doi: 10.1029/2004JB003548.

Field, E. H., G. P. Biasi, P. Bird, T. E. Dawson, K. R. Felzer, D. D. Jackson, K. M. Johnson, T. H. Jordan, C. Madden, A. J. Michael, K. R. Milner, M. T. Page, T. Parsons, P. M. Powers, B. E. Shaw, W. R. Thatcher, R. J. Weldon, and Y. Zeng (2015), Long-Term Time-Dependent probabilities for the third uniform california earthquake rupture forecast (UCERF3), *Bulletin of the Seismological Society of America*, *105*(2A), 511–543, doi: 10.1785/0120140093.

Fosdick, J. C., and K. Blisniuk (2018), Sedimentary signals of recent faulting along an old strand of the San Andreas Fault, USA, *Scientific reports*, *8*(1), 12,132, doi: 10.1038/s41598-018-30622-3.

Fuis, G. S., D. S. Scheirer, V. E. Langenheim, and M. D. Kohler (2012), A New Perspective on the Geometry of the San Andreas Fault in Southern California and Its Relationship to Lithospheric Structure, *Bulletin of the Seismological Society of America*, *102*(1), 236–251, doi: 10.1785/0120110041.

Fuis, G. S., K. Bauer, M. R. Goldman, T. Ryberg, V. E. Langenheim, D. S. Scheirer, M. J. Rymer, J. M. Stock, J. A. Hole, R. D. Catchings, R. W. Graves, and B. Aagaard (2017), Subsurface Geometry of the San Andreas Fault in Southern California: Results from the Salton Seismic Imaging Project (SSIP) and Strong Ground Motion Expectations, *Bulletin of the Seismological Society of America*, *107*(4),

1642–1662, doi: 10.1785/0120160309.

Fumal, T. E., M. J. Rymer, and G. G. Seitz (2002), Timing of Large Earthquakes since A.D. 800 on the Mission Creek Strand of the San Andreas Fault Zone at Thousand Palms Oasis, near Palm Springs, California, *Bulletin of the Seismological Society of America*, *92*(7), 2841–2860, doi: 10.1785/0120000609.

Gabrielov, A., V. Keilis-Borok, and D. D. Jackson (1996), Geometric incompatibility in a fault system, *Proceedings of the National Academy of Sciences of the United States of America*, *93*(9), 3838–3842, doi: 10.1073/pnas.93.9.3838.

Gold, P. O., W. M. Behr, D. Rood, W. D. Sharp, T. K. Rockwell, K. Kendrick, and A. Salin (2015), Holocene geologic slip rate for the Banning strand of the southern San Andreas Fault, southern California, *Journal of Geophysical Research, [Solid Earth]*, *120*(8), 5639–5663, doi: 10.1002/2015jb012004.

Gold, R. D., E. Cowgill, J. R. Arrowsmith, J. Gosse, X. Chen, and X.-F. Wang (2009), Riser diachroneity, lateral erosion, and uncertainty in rates of strike-slip faulting: A case study from Tuzidun along the Altyn Tagh Fault, NW China, *Journal of geophysical research*, *114*(B4), doi: 10.1029/2008jb005913.

Goldsby, D. L., and T. E. Tullis (2011), Flash heating leads to low frictional strength of crustal rocks at earthquake slip rates, *Science*, *334*(6053), 216–218, doi: 10.1126/science.1207902.

Gratier, J.-P., F. Renard, and P. Labaume (1999), How pressure solution creep and fracturing processes interact in the upper crust to make it behave in both a brittle and viscous manner, *Journal of Structural Geology*, *21*(8), 1189–1197, doi: 10.1016/S0191-8141(99)00035-8.

Harden, J. W., and J. C. Matti (1989), Holocene and late Pleistocene slip rates on the San Andreas fault in Yucaipa, California, using displaced alluvial-fan deposits and soil chronology, *GSA Bulletin*, *101*(9), 1107–1117, doi: 10.1130/0016-7606(1989)101<1107:HALPSR>2.3.CO;2.

Hatem, A. E., M. L. Cooke, and E. H. Madden (2015), Evolving efficiency of restraining bends within wet kaolin analog experiments, *Journal of Geophysical Research, [Solid Earth]*, *120*(3), 1975–1992, doi: 10.1002/2014jb011735.

Hatem, A. E., M. L. Cooke, and K. Toeneboehn (2017), Strain localization and evolving kinematic efficiency of initiating strike-slip faults within wet kaolin experiments, *Journal of Structural Geology*, *101*, 96–108, doi: 10.1016/j.jsg.2017.06.011.

Hatem, A. E., J. F. Dolan, R. W. Zinke, R. M. Langridge, C. P. McGuire, E. J. Rhodes, N. Brown, and R. J. Van Dissen (2020), Holocene to latest Pleistocene incremental slip rates from the east-central Hope fault (Conway segment) at Hossack Station, Marlborough fault system, South Island, New Zealand: Towards a dated path of earthquake slip along a plate boundary fault, *Geosphere*, *16*(6), 1558–1584, doi: 10.1130/GES02263.1.

Heermance, R. V., and D. Yule (2017), Holocene slip rates along the San Andreas Fault System in the San Gorgonio Pass and implications for large earthquakes in southern California, *Geophysical research letters*, *44*(11), 5391–5400, doi: 10.1002/2017GL072612.

Herbert, J. W., and M. L. Cooke (2012), Sensitivity of the Southern San Andreas Fault System to Tectonic Boundary Conditions and Fault Configurations, *Bulletin of the Seismological Society of America*, *102*(5), 2046–2062, doi: 10.1785/0120110316.

Herbert, J. W., M. L. Cooke, and S. T. Marshall (2014), Influence of fault connectivity on slip rates in southern California: Potential impact on discrepancies between geodetic derived and geologic slip rates, *Journal of Geophysical Research, [Solid Earth]*, *119*(3), 2342–2361, doi: 10.1002/2013JB010472.

Kendrick, K. J., J. C. Matti, and S. A. Mahan (2015), Late Quaternary slip history of the Mill Creek strand of the San Andreas fault in San Gorgonio Pass, southern California: The role of a subsidiary left-lateral fault in strand switching, *GSA Bulletin*, *127*(5-6), 825–849, doi: 10.1130/B31101.1.

Lin, G. (2013), Three-Dimensional Seismic Velocity Structure and Precise Earthquake Relocations in the Salton Trough, Southern California, *Bulletin of the Seismological Society of America*, *103*(5), 2694–2708, doi: 10.1785/0120120286.

Lindsey, E. O., and Y. Fialko (2013), Geodetic slip rates in the southern San Andreas Fault system: Effects of elastic heterogeneity and fault geometry, *Journal of Geophysical Research, [Solid Earth]*, *118*(2), 689–697, doi: 10.1029/2012JB009358.

Madden, E. H., M. L. Cooke, and J. McBeck (2017), Energy budget and propagation of faults via shearing and opening using work optimization, *Journal of Geophysical Research, [Solid Earth]*, *122*(8), 6757–6772, doi: 10.1002/2017jb014237.

Marshall, S. T., M. L. Cooke, and S. E. Owen (2009), Interseismic deformation associated with three-dimensional faults in the greater Los Angeles region, California, *Journal of geophysical research*, *114*(B12), doi: 10.1029/2009jb006439.

Matti, J. C., and D. M. Morton (1993), Chapter 2: Paleogeographic evolution of the san andreas fault in southern california: A reconstruction based on a new cross-fault correlation, in *The San Andreas Fault System: Displacement, Palinspastic Reconstruction, and Geologic Evolution*, vol. 178, edited by R. E. Powell, R. J. Weldon, II, and J. C. Matti, The Geological Society of America, doi: 10.1130/MEM178-p107.

Matti, J. C., D. M. Morton, and B. F. Cox (1985), Distribution and geologic relations of fault systems in the vicinity of the central Transverse Ranges, Southern California, *Tech. Rep. 85-365*, U.S. Geological Survey, doi: 10.3133/ofr85365.

McBeck, J. A., M. L. Cooke, J. W. Herbert, B. Maillot, and P. Souloumiac (2017), Work optimization predicts accretionary faulting: An integration of physical and numerical experiments, *Journal of Geophysical Research, [Solid Earth]*, *122*(9), 7485–7505, doi: 10.1002/2017jb013931.

McGill, S. F., L. A. Owen, R. J. Weldon, and K. J. Kendrick (2013), Latest Pleistocene and Holocene slip rate for the San Bernardino strand of the San Andreas fault, Plunge Creek, Southern California: Implications for strain partitioning within the southern San Andreas fault system for the last □35 k.y, *GSA Bulletin*, *125*(1-2), 48–72, doi: 10.1130/B30647.1.

McGill, S. F., L. A. Owen, R. J. Weldon, K. J. Kendrick, and R. J. Burgette (2021), Latest Quaternary slip rates of the San Bernardino strand of the San Andreas fault, southern California, from Cajon Creek to Badger Canyon, *Geosphere*, *17*(5), 1354–1381, doi: 10.1130/GES02231.1.

McPhillips, D., and K. M. Scharer (2018), Quantifying uncertainty in cumulative surface slip along the cucamonga fault, a crustal thrust fault in southern California, *Journal*

of Geophysical Research, [Solid Earth], *123*(10), 9063–9083, doi: 10.1029/2018jb016301.

Meade, B. J., and B. H. Hager (2005), Block models of crustal motion in southern California constrained by GPS measurements, *Journal of Geophysical Research, [Solid Earth]*, *110*(B3), doi: 10.1029/2004JB003209.

Morell, K. D., R. Styron, M. Stirling, J. Griffin, R. Archuleta, and T. Onur (2020), Seismic hazard analyses from geologic and geomorphic data: Current and future challenges, *Tectonics*, *39*(10), doi: 10.1029/2018tc005365.

Muñoz Zapata, J. J. (2017), Holocene geologic slip rate for the Mission Creek strand of the southern San Andreas fault, Indio Hills, Ph.D. thesis, University of Texas at Austin, doi: 10.15781/T2NP1X18Q.

Orozco, A. A. (2004), Offset of a Mid-Holocene Alluvial Fan Near Banning, CA: Constraints on the Slip Rate of the San Bernardino Strand of the San Andreas Fault, Master's thesis, California State University, Northridge.

Plesch, A., J. H. Shaw, C. Benson, W. A. Bryant, S. Carena, M. Cooke, J. Dolan, G. Fuis, E. Gath, L. Grant, E. Hauksson, T. Jordan, M. Kamerling, M. Legg, S. Lindvall, H. Magistrale, C. Nicholson, N. Niemi, M. Oskin, S. Perry, G. Planansky, T. Rockwell, P. Shearer, C. Sorlien, M. Peter Süss, J. Suppe, J. Treiman, and R. Yeats (2007), Community Fault Model (CFM) for Southern California, *Bulletin of the Seismological Society of America*, *97*(6), 1793–1802, doi: 10.1785/0120050211.

Prush, V. B., and M. E. Oskin (2020), A mechanistic erosion model for cosmogenic nuclide inheritance in single-clast exposure ages, *Earth and planetary science letters*, *535*, 116,066, doi: 10.1016/j.epsl.2020.116066.

Rittase, W. M., E. Kirby, E. McDonald, J. Douglas Walker, J. Gosse, J. Q. G. Spencer, and A. J. Herrs (2014), Temporal variations in Holocene slip rate along the central Garlock fault, Pilot Knob Valley, California, *Lithosphere*, *6*(1), 48–58, doi: 10.1130/L286.1.

Ross, Z. E., E. Hauksson, and Y. Ben-Zion (2017), Abundant off-fault seismicity and orthogonal structures in the San Jacinto fault zone, *Science advances*, *3*(3), e1601,946, doi: 10.1126/sciadv.1601946.

Scharer, K. M., D. W. Burbank, J. Chen, R. J. Weldon, C. Rubin, R. Zhao, and J. Shen (2004), Detachment folding in the Southwestern Tian Shan–Tarim foreland, China: shortening estimates and rates, *Journal of Structural Geology*, *26*(11), 2119–2137, doi: 10.1016/j.jsg.2004.02.016.

Sharp, R. V. (1981), Variable rates of Late Quaternary strike slip on the San Jacinto Fault Zone, southern California, *Journal of geophysical research*, *86*(B3), 1754, doi: 10.1029/jb086ib03p01754.

Shaw, J. H., A. Plesch, C. Tape, M. P. Suess, T. H. Jordan, G. Ely, E. Hauksson, J. Tromp, T. Tanimoto, R. Graves, K. Olsen, C. Nicholson, P. J. Maechling, C. Rivero, P. Lovely, C. M. Brankman, and J. Munster (2015), Unified structural representation of the southern California crust and upper mantle, *Earth and planetary science letters*, *415*, 1–15, doi: 10.1016/j.epsl.2015.01.016.

Styron, R. (2019), The impact of earthquake cycle variability on neotectonic and paleoseismic slip rate estimates, *Solid earth*, *10*(1), 15–25, doi: 10.5194/se-10-15-2019.

Thomas, A. L. (1993), POLU3D : A three-dimensional, polygonal element, displacement discontinuity boundary element computer program with applications to fractures, faults, and cavities in the earth's crust, Master's thesis, Stanford University.

Titus, S. J., S. Crump, Z. McGuire, E. Horsman, and B. Housen (2011), Using vertical axis rotations to characterize off-fault deformation across the San Andreas fault system, central California, *Geology*, *39*(8), 711–714, doi: 10.1130/G31802.1.

Weldon, R. J., and K. E. Sieh (1985), Holocene rate of slip and tentative recurrence interval for large earthquakes on the San Andreas fault, Cajon Pass, southern California, *GSA Bulletin*, *96*(6), 793–812, doi: 10.1130/0016-7606(1985)96<793:HROSAT>2.0.CO;2.

Wisely, B. A., and D. Schmidt (2010), Deciphering vertical deformation and poroelastic parameters in a tectonically active fault-bound aquifer using InSAR and well level data, San Bernardino basin, California, *Geophysical Journal International*, *181*(3), 1185–1200, doi: 10.1111/j.1365-246X.2010.04568.x.

Yule, D., and K. Sieh (2003), Complexities of the San Andreas fault near San Gorgonio Pass: Implications for large earthquakes, *Journal of Geophysical Research, [Solid Earth]*, *108*(B11), doi: 10.1029/2001JB000451.

Zinke, R., J. F. Dolan, E. J. Rhodes, R. Van Dissen, and C. P. McGuire (2017), Highly variable latest Pleistocene-Holocene incremental slip rates on the awatere fault at saxton river, south island, New Zealand, revealed by lidar mapping and luminescence dating, *Geophysical research letters*, *44*(22), 11,301–11,310, doi: 10.1002/2017gl075048.